Study on flow fields of centrally fuel rich swirl burner and its applications

Zhichao Chen*,,†, Zhengqi Li*, Jianping Jing*, Lizhe Chen*, Shaohua Wu*, and Yang Yao****

*School of Energy Science and Engineering, Harbin Institute of Technology, Harbin 150001, P. R. China
**Postdoctoral Station of Civil Engineering, Harbin Institute of Technology, Harbin 150090, P. R. China

Abstract−Experiments on a single-phase test facility were done to optimize primary air outlet cones of a centrally fuel rich swirl coal combustion burner. On the basis of optimized results from the single-phase test, a three-component particle-dynamics anemometer was used to measure, in the near-burner region, the characteristics of gas/particle two-phase flows for the burner with two primary air outlet cones, on a gas/particle two-phase test facility. Velocities, RMS velocities and particle volume flux profiles were obtained. According to the results, the primary air outlet cone structure of the centrally fuel rich burner was matching a 670 ton per hour boiler. The performance of the burner on a 670 ton per hour boiler was studied.

Key words: Burner, Flow Field, Coal Combustion, Utility Boiler, Gas/Particle Flow

INTRODUCTION

Much low grade coal of low calorific value is used in power plants in China. It has either a small amount of volatile matter or high moisture and/or ash content. Generally, the flame from these coals is not stable. The power industry requires coal combustion techniques that show flame stability, no slagging propensity and high combustion efficiency that also meet pollution control standards. To reduce NO_x emissions, low NO_x combustion technologies were developed [1-3]. A low NO_x burner is the most effective method for reducing NO_x emissions [5,6]. The quality of coal provided to power plants often fluctuates and is usually low grade in China. When burning low-grade coal, it is difficult for low-NO_x burners that are designed to burn high-grade coal to meet power industry requirements such as flame stability and no slagging propensity [7].

To solve the above problems, Li and co-workers [8-11] proposed a new burner, the centrally fuel rich swirl coal combustion burner (Fig. 1), in 2003. Both the inner and outer secondary airs are swirl-ing. The primary air-coal mixture duct is at the center of the burner and the primary air is non-swirling. Cone separators are installed in the primary air-coal mixture duct to concentrate the pulverized coal into the central zone of the burner.

The structure of a burner outlet affects the flow fields of single-phase and gas/particle two-phase, which is one of the most important parameters influencing the performance of a burner [12]. It is necessary to study the effects of the primary air outlet cone on flow fields of the centrally fuel rich swirl burner. A particle dynamics anemometer (PDA) is useful for simultaneous measurement of the motion of liquid and solid particles in two-phase flow [13-15]. Li et al. [12,16,17] investigated the gas/particle flows for radial bias combustion swirl burner using a three-dimensional PDA. Zhou et al. [18] investigated the effect of swirl numbers on strongly swirl-ing turbulent gas/particle flows using a three-dimensional PDA. Chen et al. [9-11] studied the influence of primary air ratio and solid concentrator on the gas/particle flows for centrally fuel rich burner and discussed the particle volume flux in different cross sections of centrally fuel rich burner, the radial bias combustion burner and volute burner.

It is virtually impossible to replicate all the physical and chemical processes of a full-sized industrial burner in a scaled down model used in research. On the other hand, it would be too expensive to do experiments in a full-sized burner. However, results from a great number of different small scale cold-flow tests compared to those of full-size burner tests show reliable predictions can be made from the scaled down model tests [19-21]. For example, Pickett et al. [21] found the velocity profiles for reacting flow showed similar trends and patterns to those observed in cold flow experiments. Thus, small scale cold flow tests were studied for centrally fuel rich burner. To validate he performance of centrally fuel rich burner, in situ industrial experiments on a 670 ton per hour boiler were studied.
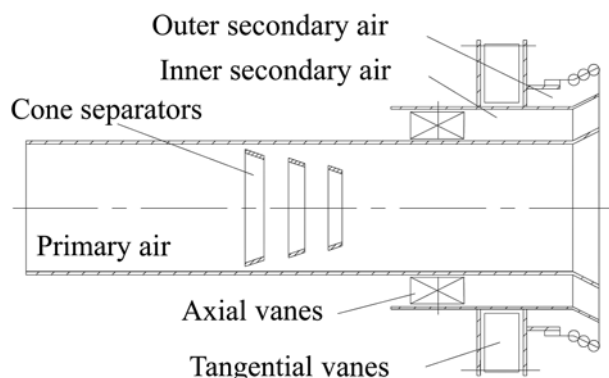
EXPERIMENTAL EQUIPMENT AND METHOD

1. Single-phase Experimental Equipment and Method
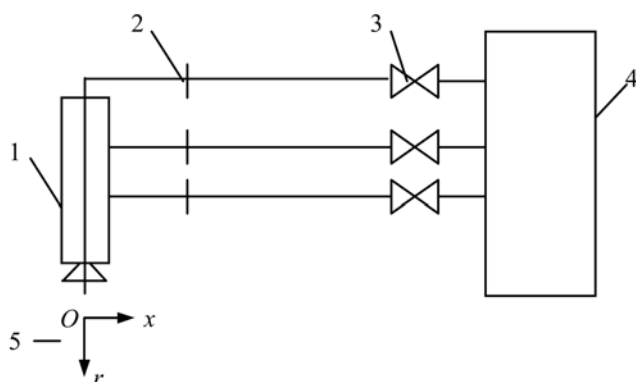The single-phase test facility, which is illustrated in Fig. 2, con-

Fig. 1. Centrally fuel rich burner.

†To whom correspondence should be addressed.
E-mail: chenzc@hit.edu.cn

Fig. 2. Schematic drawing of single-phase test facility.
  1. Model burner   4. Wind box
  2. Dynamic pressure meter   5. Coordinate frame
  3. Valve

2. Gas/Particle Two-phase Experimental Equipment and Method

A three-dimensional PDA made by Dantec was used in this study. The instrument includes an argon ion laser, a transmitter, fiber optics, receiver optics, signal processors, a traversing system, a computer system and a three-dimensional auto-coordinated rack. The PDA uses the proven phase Doppler principle for simultaneous non-intrusive and real-time measurements of three velocity components and turbulence characteristics, and makes use of new methods for phase differences between Doppler signals received by three detectors located in different positions. The instrument uses $60\times$ fiber flow optics and 57×10 PDA receiver optics. Several optical configurations from 0 to 500 mm are radially available. All instrument settings, such as bandwidth and voltage, are computer controlled. An analog-digital converter allows the computer to read the anode current of photomultipliers. The combination of photomultiplier and particle velocity correlation bias can contribute to uncertainty, but the error is likely to be small. Overall uncertainties for measured values of the mean velocity, particle diameter and particle volume flux are 1%, 4% and 30%, respectively, and the measurable ranges for size and velocity are 0.5-1,000 µm and −500 to 500 m/s, respectively.

The PDA is an instrument based on phase Doppler anemometry, which is an extension of laser Doppler anemometry (LDA). The velocity is measured from the frequency of the Doppler burst as for LDA [21]. Using PDA, the velocity, size and concentration of two-phase flow can be measured [22-25]. The main factors that determine an accurate concentration value are the setting parameters of the PDA system, the properties of particles and particle concentration. In the experiment, the degree of sphericity of glass beads employed as seeds was larger than 95%, which is advantageous in obtaining an accurate concentration. The fuel-rich primary air particle mass concentration was 0.20 kg (fuel)/kg, which corresponds to dispersed two-phase flows. Experiment indicates the PDA technique is suitable for spherical particle concentration and local flux measurements in dispersed two-phase flows [22]. In the same cross-section, the setting parameters of the PDA system are the same.

sists of wind box, valve, dynamic pressure meter, model burner and coordinate frame. In this figure r is the distance between measure point and the outlet center of model burner along radial direction and x is the distance to the exit of the burner along the jet flow direction. An air flow is induced from the wind box to the model burner. The velocities of primary air, inner secondary air and outer secondary air were adjusted by valves according to values measured by dynamic pressure meter. A coordinate frame was set in the outlet of the model burner. A thin cloth was tied in each grid of the frame. From the flow direction of the cloth, the jet borders and the central recirculation zone boundary of the burner were measured. A full industrial-scale centrally fuel rich burner studied in the experiments was designed for a 670 ton per hour coal-fired boiler. For installation in the test facility, the burner had to be scaled. The model's geometric sizes and operational parameters were obtained from scaling criteria: (1) geometric similarity, (2) secondary self-modeling flows, (3) boundary condition similarity, and (4) unaltered momentum ratios with scale reduction. A scale ratio of 1 : 4 was employed for four model burners (Fig. 3). In the figure L_1 is the length of primary air cone. To get a proper centrally fuel rich structure matching the boiler, four kinds of primary air cone structure were investigated on a single-phase test facility.
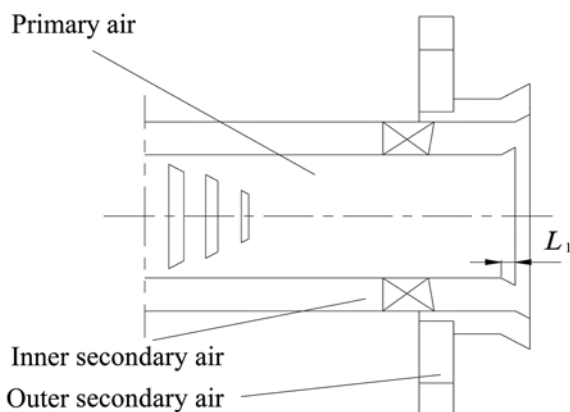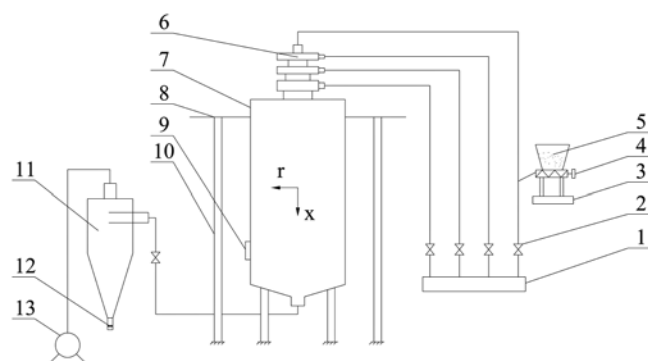

Fig. 3. Detail of the model burners' jets on the single-phase test facility.

Fig. 4. Schematic drawing of test facility.
  1. Wind box   8. Platform
  2. Valve   9. Equalizing hole
  3. Electronic scale   10. Bracket
  4. Feeder   11. Cyclone separator
  5. Particle reservoir   12. Air lock
  6. Model burner   13. Suction pump
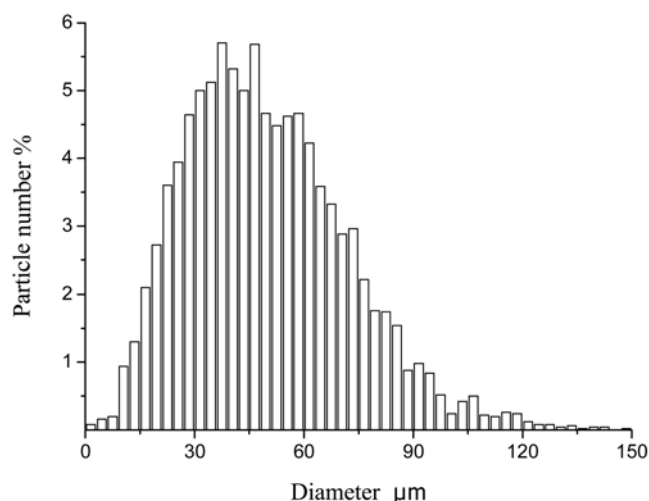 7. Test chamber

Fig. 5. Particle size distributions.

The test facility, which is illustrated in Fig. 4, consists of a suction device, feeder, model burner, test chamber and cyclone separator. An air flow is induced from the wind box to the burner by the suction device. Glass beads are fed via the feeder into the fuel rich primary air duct. The density of the glass beads used was 2,500 kg/m³. The particle size distribution obtained by the PDA is shown in Fig. 5. The mean diameter was 42 μm. Because coal particles cannot meet the steradian and reflectance characteristics required for PDA particle measurements, glass beads, which do meet these requirements, were used instead [9-12,16-18].

The full industrial-scale centrally fuel rich burner studied in the experiments was designed for a 670 ton per hour coal-fired boiler. For installation in the test facility, the burner had to be scaled. The model's geometric sizes and operational parameters were obtained by using scaling criteria: (1) geometric similarity, (2) secondary self-modeling flows, (3) boundary condition similarity, (4) material similarity, and (5) unaltered momentum ratios with scale reduction. A scale ratio of 1 : 7 was employed for two model burners (Fig. 6). On the basis of optimized results from the single-phase test, primary air outlet length (L_2) of primary air outlet cone is, respectively, 0 mm and 9.5 mm on the gas/particle two-phase test facility. No concentrator was mounted in the centrally fuel rich model burner and
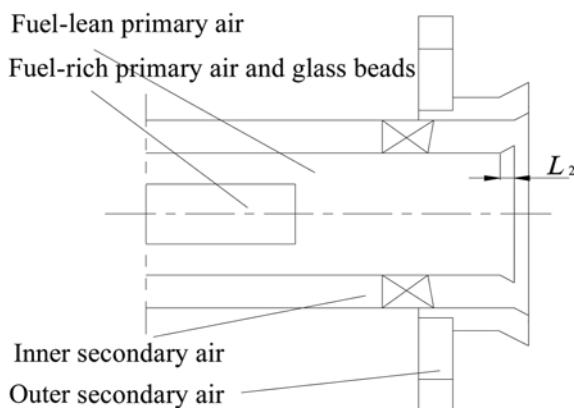

Fig. 6. Detail of the model burners' jets on two-phase test facility.

glass beads were fed only into the fuel rich duct. This simulates the extreme case in which particles in the primary air are all concentrated into the central zone of the burner. Except L_2, the structures of the two model burners are the same. The fuel-rich and fuel-lean primary air velocities were 10.0 m/s, the inner secondary air velocity was 10.58 m/s, and the outer secondary air velocity for both burners was 16.07 m/s. The primary air particle mass concentration, which is defined as the ratio of particle mass flow rate to primary air mass flow rate, was 0.20 kg (fuel)/kg (air).

During the experiment some of the smaller particles were lost due to the low efficiency of the cyclone separator. The particle material had to be frequently renewed to maintain the same particle size distribution as closely as possible. The ratio of the test chamber diameter to the nozzle diameter of the outer secondary air outflow was 4.83. Ratios greater than 3 are considered to be low-confinement flows [26]. Particles with diameters of 0-8 μm were used to trace the air flow, and particles with diameters of 10-100 μm were used to represent the particle phase flow. Particles with diameters of 0-100 μm were used for analysis of the particle volume flux and normalized particle number concentration. Because of uncertainties in the determination of the cross-section of the control volume, the measured mass flux was corrected by using the global mass balance. Therefore, the total particle mass flow rate at the inlet was obtained by integrating the mass flux profile. The global mass flow rate was obtained by weighing particles collected during a certain time period. In addition, a correction factor was applied to the mass flux measurements for all other cross-sections [9-12,16,17,26].

3. In Situ Industrial Experimental Equipment and Method

A 670 ton per hour boiler of B&WB-670/13.7-M type was made by Babcock & Wilcox Beijing CO. LTD. It is fired with pulverized coal and synchronized to a 200 MW$_e$ steam generator. The boiler was equipped with 18 EI-DR burners. It is a dry-ash type furnace. The boiler was equipped with the coal pulverizing storage system in which pulverized coal is conveyed by hot air. Burning low-grade coal the boiler only operates stably at 140 MWe without auxiliary fuel oil. The boiler with 18 EI-DR burners had to burn 2,000 ton auxiliary fuel oil a year with the purpose of keeping a stable flame. Table 1 shows proximate analysis of the low-grade coal. During five months (Mar.-Jun. and Nov., 2005) the statistical proximate analysis of coals used in the boiler were obtained.

To solve the above problems, six EI-DR burners at the bottom row were retrofitted by the centrally fuel rich burners. To study the performance of the centrally fuel rich burner, in situ industrial experiments were conducted.

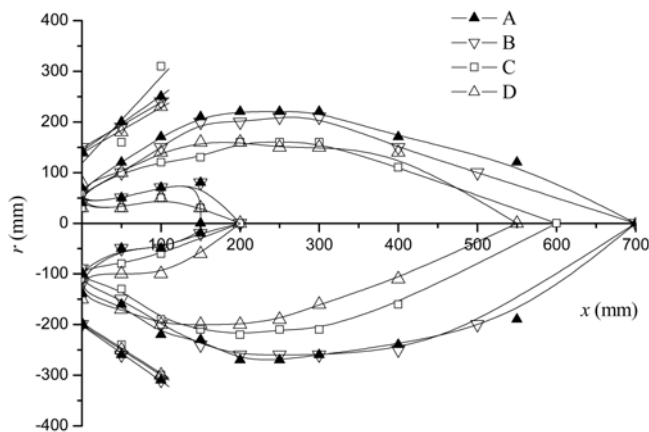### RESULTS AND DISCUSSION

1. Single-phase Tests

The mass flow rate of the primary, inner secondary air and the outer secondary air was calculated based on the similarity criteria. Table 2 shows single-phase experimental parameters and results for four lengths of primary air outlet cones. In this table r_1, r_{2n} and r_{2w}, respectively, is the ratio for primary air, inner secondary air and outer secondary air. v_1, v_{2n} and v_{2w}, respectively, are velocity for primary air, inner secondary air and outer secondary air. L_h and D_h, respectively, are length and the largest diameter of the central recirculation zone. γ is the divergent angle of the air jet. d_1 is the dia-

Table 1. The statistical proximate analysis of coals

			Mar.	Apr.	May	Jun.	Nov.
Average value	Moisture, %		2.91	3.02	3.04	2.8	3.02
	Ash, %		35.95	36.43	35.21	35.1	43.28
	Volatile matter, %		11.28	11.34	11.32	11.7	11.48
	Fixed carbon, %		49.86	49.21	50.43	50.4	42.22
	Net heating value, kJ kg^{-1}		18991	18381	19408	19681	15623
A fluctuant range	Moisture, %	Max.	6.2	5.6	5.4	5.4	6.0
		Min.	3.6	3.6	3.6	3.6	3.6
	Ash, %	Max.	49.32	46.42	44.36	48.46	57.19
		Min.	25.64	21.55	27.40	26.67	32.80
	Volatile matter, %	Max.	13.81	13.75	13.22	16.71	13.85
		Min.	10.01	10.20	10.01	10.18	10.14
	Net heating value, kJ kg^{-1}	Max.	23686	23470	22705	23476	21181
		Min.	12831	13684	16686	14791	10279

Table 2. Single-phase experimental parameters and results

Case	L_1 (mm)	r_1 (%)	r_{2n} (%)	r_{2w} (%)	u_1 (m/s)	u_{2n} (m/s)	u_{2w} (m/s)	L_h/d_1	D_h/d_1	γ (°)
A	0	27.51	40	60	11.59	12.54	18.61	2.30	1.61	95.45
B	16	27.51	40	60	11.59	12.54	18.61	2.30	1.55	89.71
C	25	27.51	40	60	11.59	12.54	18.61	1.97	1.28	104.5
D	33	27.51	40	60	11.59	12.54	18.61	1.81	1.18	86.99

Fig. 7. Jet border and central recirculation zone boundary of centrally fuel rich burner with different length of primary air outlet cone.

Fig. 8. Profiles of mean axial velocities for the two model burners.

meter of the outer secondary air duct which is 304 mm.

Fig. 7 shows the jet border and the central recirculation zone boundary of centrally fuel rich burner with different cases. Up to a jet distance of $x/d_1=0.33$, jet borders of the air form almost a straight line. To show the jet development, the divergent angle of the air jet is defined as the angle between the air jet borders at the section from $x/d_1=0$ to 0.33. The distance between the two measurements traversed is 50 mm.

As L_1 decreases, the length and the largest diameter of the central recirculation zone increases. D_h/d_1 for case C and D is smaller than 1.3. According to experience in a swirl burner, the central recirculation zones for case C and D are too small to keep a stable flame. L_h/d_1 for case A and B is the same. D_h/d_1 for case A and B

is bigger than 1.3, and the difference for D_h/d_1 between case A and B is small. Thus, the length of primary air outlet cone for case A ($L_1=0$ mm) and B ($L_1=0$ mm) may keep a stable flame.

2. Gas/Particle Two-phase Tests

To further investigate the single-phase test results (the structure for case A and case B), gas/particle flow characteristics were measured for cross-sections of $x/d_2=0.1$, 0.3, 0.5, 0.7, 1.0, 1.5, and 2.5, where x is the distance to the exit of the burner along the jet flow direction (Fig. 4) and d_2 is the diameter of the outer secondary air duct, which is 176 mm.

2-1. Gas/Particle Velocities

Fig. 8 shows profiles of the gas/particle mean axial velocities for the two model burners. From the burner jet to the $x/d_2=0.3$ cross-sections, there are two peaks in the profiles: the peak near the chamber axis is the primary flow zone for the gas/particle mixture, and

the other near the wall is the secondary airflow zone. The peak near the chamber axis is greater than that near the wall. With diffusion of the primary gas/particle mixture into the secondary air and diffusion of the secondary air towards the wall, both peaks gradually decrease and the peak value near the wall moves towards the wall.

The primary gas/particle mixture for two model burners partially penetrates the central recirculation zone and is then deflected radially. In the cross-sections of x/d_2=0.1-0.5, in the radius range 0-20 mm, the gas/particle mean axial velocities for the burner with L_2=9.5 mm are larger than those with L_2=0 mm. The degree of penetration (how far the primary air penetrates the central recirculation zone) for the burner with L_2=9.5 mm is higher than that for the burner with L_2=0 mm.

Compared with the burner with L_2=9.5 mm, the peak near the wall for the burner with L_2=0 mm is lower. From the burner jet to the x/d_2=1.5 cross-sections, the gas/particle velocities near the wall for the burner with α=0° are larger. From the burner jet to the x/d_2=0.7 cross-sections, the gas/particle velocities of backflows are larger and the central recirculation zone is closer to the chamber axis. With L_2=0 mm the mixing of primary air and inner secondary air has progressed more, resulting in the peak near the wall decreasing quickly and a larger negative pressure forming near the chamber axis. This structure of the burner is able to form a bigger central recirculation zone more easily. The primary air total momenta of the two model burners are identical. With the development of the burner jet, the influence of the difference of primary air outlet angle for the burner on the gas/particle mean axial velocities is small. In the cross-section of x/d_2=2.5, profiles of the gas/particle mean axial velocities for the two burners are similar.

Fig. 9 shows profiles of the gas/particle mean radial velocities for the two model burners. From the burner jet to the x/d_2=0.7 section, the profiles show two peaks: the peak near the chamber axis is the primary gas/particle mixture flow zone, and the other near the wall is the secondary air flow zone. The peak near the wall is always greater than the peak near the chamber axis. With diffusion of the primary gas/particle mixture into the secondary air and diffusion of the secondary air towards the wall, the two peaks move towards the wall. With the development of the burner jet, the influence of two primary air outlet cones on the gas/particle mean radial velocities is small. Profiles of the gas/particle mean radial
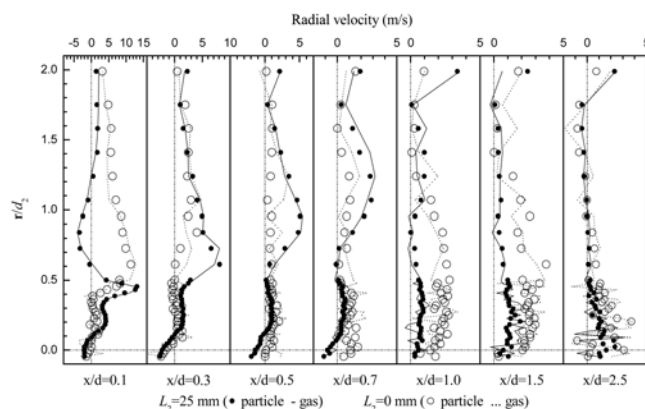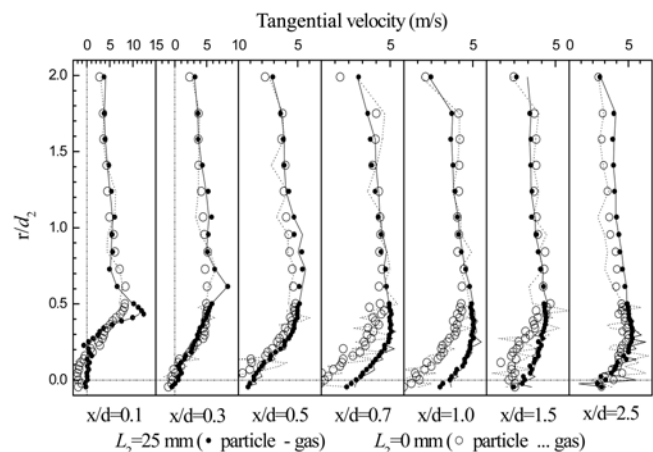

Fig. 10. Profiles of mean tangential velocities for the two model burners.

velocities for the two model burners are similar. Compared with L_2=9.5 mm, in the cross-section x/d_2=0.1, for the radius from 40 mm to R, the gas/particle mean radial velocities with L_2=0 mm are smaller; for the radius from R to 180 mm, the gas/particle mean radial velocities with L_2=0 mm are larger. In the cross-section x/d_2=0.3-0.7, the peak near the wall with L_2=0 mm is smaller. This phenomenon occurs because, with L_2=0 mm, the mixture between primary air and inner secondary air is more progressed and a larger negative pressure forms near the chamber axis. Profiles of the gas/particle RMS radial velocities with two primary air outlet cones are similar.

Fig. 10 shows profiles of the gas/particle mean tangential velocities for the two model burners. As the primary air is non-swirling, the mean tangential velocities for the burners are relatively small in the x/d_2=0.1 cross-section (r≤40 mm). Downstream from the x/d_2=0.5 cross-section, the peak mean tangential velocities move towards the chamber axis, which indicates the gas/particle mixture near the chamber axis begins to swirl, driven by secondary air. Compared with L_2=0 mm, in the x/d_2=0.3 cross-section, the distribution of the mean tangential velocities for the burner with L_2=9.5 mm is a Rankine-type vortex, which is a combination of a solid-body rotational core and a free vortex. This phenomenon occurs because, with L_2=0 mm, the mixture between primary air and inner secondary air has progressed more and a larger negative pressure forms near the chamber axis. With the development of the burner jet, the influence of the length of primary air outlet cone on the gas/particle mean tangential velocities is small. Profiles of the gas/particle mean tangential velocities for the two burners are similar. With diffusion of the secondary air towards the wall, the peaks gradually decrease and move towards the wall.

2-2. Particle Volume Flux

Fig. 11 shows profiles of the particle volume flux from 0-100 μm in different cross-sections for the two model burners, all of which have back flows near the wall. In the four cross-sections from x/d_2=0.1-0.7, the profiles of particle volume flux have two peaks. With movement of the secondary air towards the wall, the two peaks gradually decrease and the peak near the wall moves towards the wall. The peak near the chamber axis is the primary gas/particle mixture flow zone, and the other near the wall is the secondary airflow zone. For the two burners, the primary gas/particle mixture partially pene-
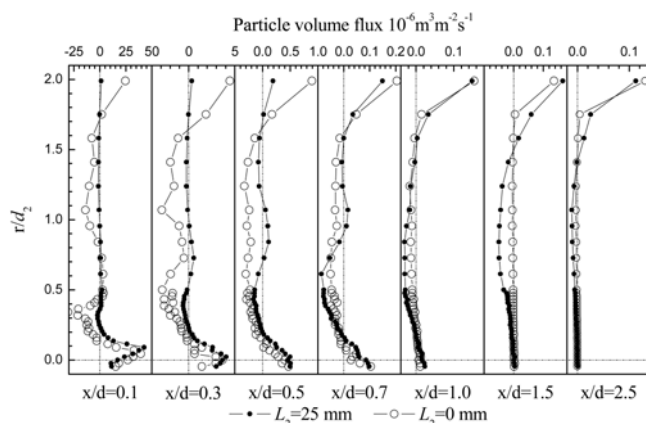

Fig. 9. Profiles of mean radial velocities for the two model burners.

Fig. 11. Particle volume flux profiles for the two model burners.

trates the central recirculation zone and is then deflected radially.

For the burner with L_2=9.5 mm, in the three cross-sections from x/d_2=0.1-0.5, the peak near the chamber axis is always larger than particle volume flux in the other position. For the burner with L_2=0 mm, in the six cross-sections from x/d_2=0.3-2.5, the particle volume flux near the wall is always larger than that in other positions. Compared with L_2=9.5 mm, the particle volume flux peak with L_2=0 mm near the chamber axis is smaller in all cross-sections. The peak with L_2=0 mm near the chamber axis decreases quickly and is negative in the cross-section x/d_2=0.5. In the three cross-sections from x/d_2=0.3-0.7, the particle volume flux with L_2=0 mm in the central recirculation zone is much larger than that with L_2=9.5 mm. In the three cross-sections from x/d_2=1.0-2.5, the particle volume flux in the central recirculation zone with L_2=9.5 mm is much larger than that with L_2=0 mm. This phenomenon occurs because the mixing of primary air and inner secondary air is more progressed with L_2=0 mm. The particles are easily diffused to secondary air.

2-3. Influence of Gas-particle Flow Characteristics on Combustion

The particle residence time in the burner's central recirculation zone affects particle burnout in the burner region. For centrally fuel rich burners with two primary air outlet cones, the primary gas-particle mixture partially penetrates the central recirculation zone and is then deflected radially. The residence time of particles in the reducing atmosphere is prolonged. Pulverized coal is concentrated in the central zone of the burner and thus a zone of high temperature and high fuel concentration is formed. With increasing fuel concentration, the degree of blackness of the fuel stream increases. When radiation heat, which is absorbed from the high-temperature flame of the furnace, then increases, the gas temperature increases. Near the chamber axis, there is a large particle volume flux, high gas temperature, which exhibits intense heat convection with the central recirculation zone. This is advantageous for coal heating, firing and flame stability. The particle volume flux is large at the center of the test chamber, and large particles are mainly resident in the burner's central recirculation zone, where the temperature is high. Thus, a centrally fuel rich burner is advantageous for burnout and producing a stable flame. With L_2=0 mm, air and particles mix intensively in the forepart. Compared with the burner with L_2=0 mm, with L_2=9.5 mm the air and particles mix intensively at a later time. When burning pulverized coal with high volatile matter, it is better to adopt

a burner with L_2=9.5 mm. To burn pulverized coal with low volatile matter, the centrally fuel rich burner with L_2=0 mm is more suitable than a burner with L_2=9.5 mm.

With two primary air outlet cones, the particle volume flux is large in the central recirculation zone and the primary gas-particle mixture partially penetrates the central recirculation zone and is then deflected radially. The central recirculation zone consists of hot burned gases with a low amount of O_2. Devolatilization occurs in the zone and hydrocarbons compete with nitrogen for the available substoichiometric O_2. In this reducing environment, NO formation is low and most of the reactive nitrogen is converted to N_2. This inhibits the formation of fuel-NO_x. Staged mixing of the secondary air decreases the temperature in the near-burner region, which reduces the amount of thermal NO simultaneously with fuel nitrogen-derived NO.

Particles are ejected from the center of the centrally fuel rich burner and have small tangential and radial velocities, with major particles gathering in the burner's central zone. This is beneficial for the formation of an oxidizing atmosphere near the water-cooled wall, which increases the ash fusion point, and for resisting slagging and high-temperature corrosion.

3. In Situ Industrial Cold Flow Experiments

On the basis of optimized results from the single-phase test and gas/particle two-phase test, the length of primary air outlet cone of centrally fuel rich burner on the 670 ton per hour was optimized to be 0 mm. From in situ industrial cold flow experiments, we can analyze and predict the characteristics of the flame. If the central recirculation zone of a burner is small, it is difficult to draw enough high temperature gas to keep a stable flame. If the extremely large central recirculation zone and divergent angle of the air jet of burners were formed, the airflow field of the two adjacent burners would be influencing each other. That works against keeping a stable flame. So it is important that a burner has a moderate central recirculation zone and divergent angle of the air jet.

In the cold flow experiments, a coordinate frame was set in the outlet of the burner. A narrow thin cloth was tied in each grid of the frame. From the flow direction of the cloth, the jet borders and the central recirculation zone boundary of the burner were measured. The mass flow rate of the primary, the inner secondary air and the outer secondary air was calculated based on the similarity criteria. Table 3 shows in situ industrial cold flow experimental parameters of centrally fuel rich burner on a 670 ton per hour boiler. In this table d_3 is the diameter of the outer secondary air duct, which is 1,216 mm.

Fig. 12 shows the jet border and the central recirculation zone boundary of centrally fuel rich burner on a 670 ton per hour boiler. In the figure, x is the distance between the measured point and the water cooled wall. Up to a jet distance of x/d_3=0.42, jet borders of the air form almost a straight line. To show the jet development, the divergent angle of the air jet is defined as the angle between the air jet borders at the section from x/d_3=0 to 0.42. The distance between the two measurements traversed was 100 mm. From the figure, we

Table 3. In situ industrial cold flow experimental parameters of centrally fuel rich burner on 670 ton per hour boiler

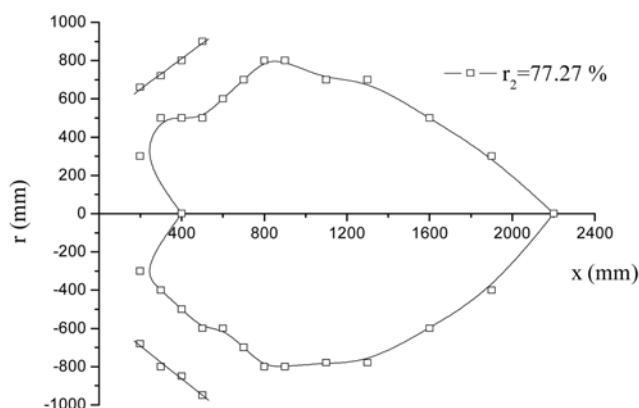| u_1 (m/s)	u_{2x} (m/s)	u_{2z} (m/s)	r_1 (%)	r_2 (%)	L_h/d_3 (%)	D_h/d_3 (%)	Å (°)
9.79	16.5	20.1	22.73	77.27	1.84	1.34	79.4

Fig. 12. The jet border and the central recirculation zone boundary of the centrally fuel rich burner.

can see that centrally fuel rich burner has a moderate central recirculation zone to keep a stable flame.

4. In Situ Industrial Reacting Flow Experiments
4-1. Pulverized Coal Burn-out and Flame Stability

Table 4 shows the parameters and results of the boiler thermal efficiency. After six burners at the bottom row were retrofitted, a thermal efficiency test of the boiler with 18 EIDR burners was conducted. The boiler can run stably at a load of 200 MW$_e$. The test showed that the parameters and the load of the boiler met the designed requirements. The thermal efficiency of the boiler was 91.11% and increased 0.51%.

A low load test of the boiler with the six centrally fuel rich burners was conducted when burning random coal (Table 5). At the beginning of the test, pulverized coal fed to the burners in the top row was reduced. When the load on the boiler reduced to 130 MW$_e$,

six burners in the top row and two burners in the middle row of the rear wall were out of service in sequence. Then, the boiler operated stably at a load of 100 MW$_e$ without auxiliary oil. The temperature and the pressure of the main stream were 544 °C and 9.6 MPa. Furnace pressure fluctuation was ±50 Pa. The average flame temperature in the burners region was 1,015 °C. The flame scanners showed a steady signal rather than an intermittent signal, and the boiler ran well. The low load test lasted for 3 h. The turn-down ratio was 45%. After centrally fuel rich burners were adopted, flame stability was greatly improved and no flame extinction occurred even with a wide variation in coal quality and boiler load.

4-2. NO$_x$ Emissions

When thermal efficiency tests of the boiler were conducted, NO$_x$ emissions were measured at the same time. Before six burners at the bottom row were retrofitted, NO$_x$ emissions were 961 mg/m^3 @6% O$_2$. After six burners at the bottom row were retrofitted by centrally fuel rich burners, NO$_x$ emissions were 795 mg/m^3 @6% O$_2$. With six centrally fuel rich burners, NO$_x$ emissions were reduced 166 mg/m^3 @6% O$_2$ and the reduced ratio was 17.27%.

4-3. Slagging and High-temperature Corrosion

After six burners at the bottom row were retrofitted by centrally fuel rich burners, no slagging and high-temperature corrosion in the furnace happened. Particles were ejected from the center of the centrally fuel rich burner and had small tangential and radial velocities, with major particles gathering in the burner's central zone. This is beneficial for the formation of an oxidizing atmosphere near the water-cooled wall, which increases the ash fusion point, and for resisting slagging and high-temperature corrosion.

CONCLUSIONS

As the length of the primary air outlet cone decreases, length and

Table 4. Parameters and results of boiler thermal efficiency

	Before eight burners at the bottom row were retrofitted	After eight burners at the bottom row were retrofitted
Fixed carbon (% as received)	45.31	48.45
Hydrogen (% as received)	2.98	2.69
Oxygen (% as received)	2.71	3.77
Nitrogen (% as received)	0.75	0.68
Sulfur (% as received)	1.59	1.74
Moisture (% as received)	5.7	7.39
Ash (% as received)	40.96	35.28
Volatile matter (% as dry ash free)	27.63	22.86
Net heating value (kJ kg^{-1} as received)	16050	18130
The boiler thermal efficiency (%)	90.50	91.11

Table 5. The ultimate and proximate analysis of coals

Description		Description	
Fixed carbon (% as received)	56.90	Sulfur (% as received)	1.10
Hydrogen (% as received)	2.46	Moisture (% as received)	7.40
Oxygen (% as received)	2.53	Ash (% as received)	28.75
Nitrogen (% as received)	0.86	Volatile matter (% as dry ash free)	16.08
Net heating value (kJ kg^{-1} as received)	20920		

the largest diameter the central recirculation zone increase.

The primary gas-particle mixture of centrally fuel rich burner partially penetrates the central recirculation zone and is then deflected radially. For the model burner with L_2=9.5 mm, in the three cross-sections from x/d_2=0.1-0.5, the peak near the chamber axis is always larger than particle volume flux in the other position. For the burner with L_2=0 mm, in the six cross-sections from x/d_2=0.3-2.5, the particle volume flux near the wall is always larger than that in the other position. Compared with L_2=9.5 mm, the particle volume flux peak with L_2=0 mm near the chamber axis is smaller in all cross-sections. Compared with the centrally fuel rich burner with L_2=0 mm, in the x/d_2=0.3 cross-section, the distribution of the mean tangential velocities for the burner with L_2=9.5 mm is a Rankine-type vortex.

A centrally fuel rich swirl coal combustion technology was developed to burn low grade coal with low NO_x emissions for 670 ton per hour boiler. Six EIDR burners in the bottom row were retrofitted with the new burners. A centrally fuel rich burner can form a moderate central recirculation zone. The boiler can run stably at a load of 200 MW_e. With the centrally fuel rich burners on the bottom row, the boiler operated stably at 100 MW_e without auxiliary fuel oil. With six centrally fuel rich burners, NO_x emissions were 795 mg/m^3 @6% O_2. The NO_x emissions were reduced 166 mg/m^3@6% O_2 and the decreased ratio was 17.27%. With centrally fuel rich burners, flame stability was greatly improved; no flame extinction occurred even with a wide variation in coal quality and boiler load, no slagging and high-temperature corrosion in the furnace occurred.

ACKNOWLEDGMENTS

NOMENCLATURE

d_1 : the diameter of the outer secondary air duct (304 mm)
d_2 : the diameter of the outer secondary air duct (176 mm)
d_3 : the diameter of the outer secondary air duct (1,216 mm)
D_h : the largest diameter the central recirculation zone
L_1 : the length of primary air cone for single-phase test
L_2 : the length of primary air cone for gas/particle two-phase test
L_h : the length of the central recirculation zone
r : the distance between measure point and the center line of burner along radial direction
r_1 : the ratio for primary air
r_{2n} : the ratio for inner secondary air
r_{2w} : the ratio for outer secondary air
v_1 : the velocity for primary air
v_{2n} : the velocity for inner secondary air
v_{2w} : the velocity for outer secondary air
x : the distance to the exit of the burner along the jet flow direction

γ : the divergent angle of the air jet

REFERENCES

1. P. H. Qiu, S. H. Wu, S. Z. Sun, H. Liu, L. B. Yang and G. Z. Wang, *Korean J. Chem. Eng.*, **24**, 683 (2007).
2. X. Jun, X. X. Sun, S. Hu and D. X. Yu, *Fuel Process. Technol.*, **68**, 139 (2000).
3. B. J. Zhong, W. W. Shi and W. B. Fu, *Fuel Process. Technol.*, **79**, 93 (2002).
4. L. K. Huang, Z. Q. Li, R. Sun and J. Zhou, *Fuel Process. Technol.*, **87**, 363 (2006).
5. W. C. Kil, S. P. Heung and K. L. Yong, *Korean J. Chem. Eng.*, **10**, 140 (1993).
6. S. C. Kim and Y. N. Chun, *Korean J. Chem. Eng.*, **25**, 73 (2008).
7. D. P. Rees, L. D. Smoot and P. O. Hedman, *18th International symposium on combustion*, *The combustion institute*, 1305 (1981).
8. Z. Q. Li, Z. C. Chen, R. Sun and S. H. Wu, *Journal of the Energy Institute*, **80**, 123 (2007).
9. Z. C. Chen, Z. Q Li., F. Q. Wang, J. P. Jing, L. Z. Chen and S. H. Wu, *Fuel*, **87**, 2102 (2008).
10. Z. C. Chen, Z. Q. Li, J. P. Jing, F. Q. Wang, L. Z. Chen and S. H. Wu, *Fuel Process. Technol*, DOI:10.1016/j.fuproc.2008.03.005.
11. Z. C. Chen, Z. Q. Li, J. P. Jing, H. D. Wei, L. Z. Chen, S. H. Wu and Y. Yao, *International Journal of Chemical Reactor Engineering*, **6**: A39, Available at: http://www.bepress.com/ijcre/vol6/A39 (2008).
12. Z. Q. Li, Z. X. Wan, R. Sun, S. Z. Sun, L. Z. Chen, S. H. Wu and Y. K. Qin, *Energy*, **27**, 1119 (2002).
13. G. Q. Dai, W. M. Chen, J. M. Li and L. Y. Chu, *Chem. Eng. J.*, **74**, 211 (1999).
14. J. Bao and S. L. Soo, *Powder Technology*, **85**, 261 (1995).
15. Z. C. Lin, W. D. Fan, Y. Y. Li, Y. H. Li and M. C. Zhang, *Energy & Fuels*, DOI: 10.1021/ef800896z (2009).
16. Z. Q. Li, R. Sun, L. Z. Chen, Z. X. Wan, S. H. Wu and Y. K. Qin, *Fuel*, **81**, 829 (2002).
17. Z. Q. Li, R. Sun, Z. X. Wan, S. Z. Sun, S. H. Wu and Y. K. Qin, *Combust. Sci. Technol.*, **175**, 1979 (2003).
18. L. X. Zhou, Y. Li, T. Chen and Y. Xu, *Powder Technology*, **112**, 79 (2000).
19. R. Weber, *Proceedings of the 26th international symposium on combustion*, **2**, 3343 (1996).
20. D. Shin, S. Park, B. Jeon, T. Yu and J. Hwang, *J. Mech. Sci. Technol.*, **20**, 2310 (2006).
21. L. M. Pickett, R. E. Jackson and D. R. Tree, *Combust. Sci. Technol.*, **143**, 79 (1999).
22. L. Aísa, J. A. Garcia, L. M. Cerecedo, P. I. García and E. Calvo, *Int. J. Multiphase Flow*, **28**, 301 (2002).
23. S. Moon, C. Bae, J. Choi and E. Abo-Serie, *Fuel*, **86**, 400 (2007).
24. A. W. Hübner, M. J. Tummers, K. Hanjaliæ and T. H. van der Meer, *Thermal. Fluid Sci.*, **27**, 481 (2003).
25. M Sommerfeld and H. H. Qiu, *Int. J. Heat and Fluid Flow*, **12**, 20 (1991).
26. R. Weber, B. M. Visser and F. Bousan, *Int. J. Heat and Fluid Flow*, **11**, 225 (1990).